TECHNICAL UNIVERSITY OF CLUJ-NAPOCA

ACTA TECHNICA NAPOCENSIS

Series: Applied Mathematics, Mechanics, and Engineering
Vol. 67, Issue IV, November, 2024

ANALYSIS OF THE THERMAL EXPANSION COEFFICIENT OF ANISOTROPIC SOLIDS: APPLICATION TO CALCIUM SILICATE – PART II – EVALUATION OF THE EXPERIMENTAL DATA

Adrian-Ioan BOTEAN

Abstract: *This paper aims determining the linear thermal expansion coefficient (CTE) of calcium silicate using an optical method for measuring deformations called digital image correlation method (DIC). DIC provides full-field in-plane deformation fields of the test planar specimen surface by comparing the digital images of the specimen surface acquired before and after deformation. The samples evaluated in this paper are two calcium silicate plates: a square one (with sides of 50x50 mm and 3 mm of thickness) and a circular one (with a diameter of 50 mm and a thickness of 3 mm). The measuring set-up developed includes a simple heating device, thermal sensors and a thermo-camera for real-time temperature measurement and monitoring of the sample and a 2D and 3D-DIC measuring system. The study is carried out during two stages: Part I – Introduction to the measurement methodology and Part II – Evaluation of the experimental data.*

Key words: *thermal expansion coefficient (CTE), thermal displacement, calcium silicate, digital image correlation (DIC).*

1. INTRODUCTION

Experimental measurements of temperature are conducted at both the upper and lower facets of the specimens under consideration, which include circular and square plates. This is accomplished using the FLIR T400 thermal imaging camera alongside Pt100 thermoresistive transducers, supported by the Spider 8 Data Acquisition System and CatmanEasy Software from HBM. A total of five distinct sets of tests have been carried out, labeled as Set 1, Set 2, and so on up to Set 5. Each of these sets comprises between 32 and 36 measurements, capturing temperature variations within a range of 20 to 110 °C, taken at intervals of 30 seconds.

From the collected data, two key temperature gradients are calculated: Δt', which represents the temperature difference between the lower and upper facets at the final heating state, and Δts, which indicates the temperature gradient observed at the upper face when comparing the final state to the initial state of heating. Following this, the average values for these gradients, Δt' and Δts, are determined across the five sets of experimental data obtained.

In conjunction with the temperature field measurements, a speckle pattern on the surface of the target specimens is captured using the Q400 System. By correlating these recorded images with a reference image, it becomes possible to ascertain the sizes of the linear deformations, denoted as dx and dy, relative to the defined reference axes (x and y). These deformations are assessed under three different working scenarios: first, the evaluation of dx and dy deformations is performed using CCD1; second, the analysis is carried out using CCD2; and third, a comprehensive evaluation of both dx and dy deformations is undertaken through the combined use of both CCDs, known as 3D Digital Image Correlation (DIC). Finally, based on the data obtained, average values are computed for the three scenarios under consideration, providing a comprehensive understanding of the thermal and deformation behaviors of the specimens.

Received: 30.09.24; **Similarities**: 24.11.24: **Reviewed**: 05.11./07.10.24: **Accepted**:25.11.24.

2.EXPERIMENTAL AND THEORETICAL PROCEDURE

In the next stage of the study, we aim to determine the specific linear deformation induced by the temperature gradient. This is achieved through the application of specific mathematical relationships that relate temperature changes to linear deformations. The following equations are utilized to quantify these deformations:

$$\varepsilon_x = \frac{dx}{50};\ \varepsilon_y = \frac{dy}{50} \quad (1)$$

where 50 represents the length unit that defines the diameter or side of the analyzed samples (dimensions expressed in millimeters).

Thus, knowing the size of the temperature gradient ($\Delta t'$ or Δt_s) in relation to which the samples deform in relation to the axes of the reference system x and y, the CTE (denoted by α) is calculated using the following relations:

$$\alpha_x = \frac{\varepsilon_x}{\Delta t'(\Delta ts)};\ \alpha_y = \frac{\varepsilon_y}{\Delta t'(\Delta ts)} \quad (2)$$

It is evident that the accuracy of the measured coefficient of thermal expansion (CTE) for the specimens under consideration is fundamentally dependent on two key factors: the precision of the thermal expansion displacements computed using the Digital Image Correlation (DIC) technique, and the accuracy of the temperature measurements obtained from the thermal sensors [1].

The DIC technique relies on capturing high-resolution images of the specimen's surface as it undergoes thermal expansion. The accuracy of the displacement measurements—critical for calculating the CTE—depends on the quality of the speckle pattern, the resolution of the imaging system, and the effectiveness of the correlation algorithms used. Any inaccuracies in these measurements can directly affect the calculated values of linear deformation and, consequently, the CTE [2].

The reliability of temperature readings is equally important. The temperature sensors employed, such as the Pt100 thermoresistive transducers, must provide precise and consistent measurements across the specified temperature range. Factors such as sensor calibration, placement, and response time can significantly influence the accuracy of the temperature data. Any discrepancies in temperature measurement will lead to errors in the calculated thermal gradients, ultimately impacting the assessment of thermal expansion [3].

In summary, both the accuracy of the thermal expansion displacements obtained through the DIC method and the reliability of the temperature measurements are critical for ensuring the precision of the CTE values for the specimens [4]. Addressing potential sources of error in both measurement processes will enhance the overall validity of the results and conclusions drawn from the study.

3. RESULTS AND DISCUSSIONS

In accordance with the stages presented in detail in the previous paragraph in Figure 1, Figure 2 and Figure 3 are drawn the temperature gradient variation diagrams Δt_s and $\Delta t'$ determined according to the data provided by the thermal imaging camera FLIR T400 and the Pt100 thermoresistances (according to Figure 13 and Figure 14 from Part 1 - Introduction to the measurement methodology) for the circular model.

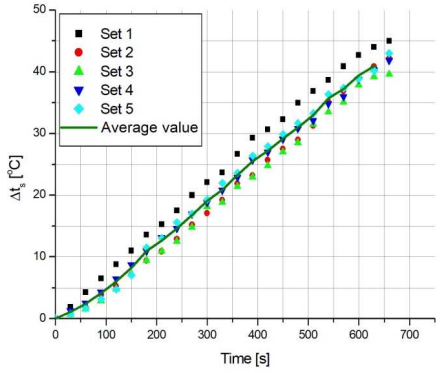

Fig. 1. Variation diagram of the temperature gradient **Δts** (the temperature gradient at the level of the upper face corresponding to the final and initial state of heating) as a function of time for the circular model.

Average values are represented in the same diagram according to Figure 4.

In Figure 5, Figure 6 and Figure 7, the temperature gradient variation diagrams Δts and Δt' determined according to the data provided by the FLIR T400 thermal imaging camera and Pt100 thermoresistances (according to Figure 13 and Figure 14 from Part 1 - Introduction to the

measurement methodology) for the quadratic model.

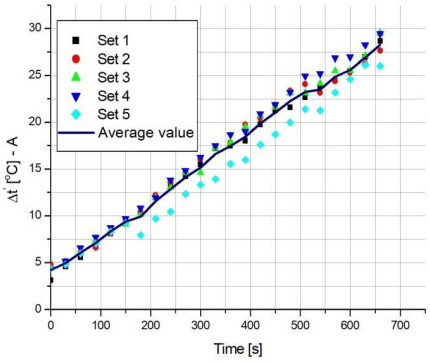

Fig. 2. Variation diagram of the temperature gradient **Δt'** (the temperature gradient between the lower and the upper facet for the final state of heating) as a function of time for the circular model (according to Figure 20 from Part 1 - Introduction to the measurement methodology).

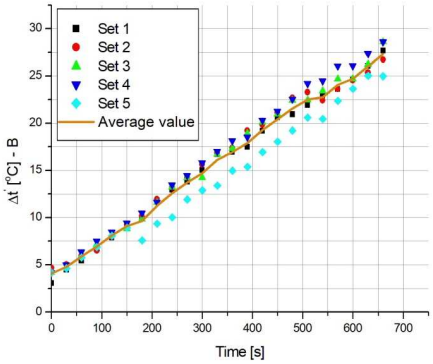

Fig. 3. Variation diagram of the temperature gradient Δt' (the temperature gradient between the lower and the upper facet for the final state of heating) as a function of time for the circular model (according to Figure 20 - from Part 1 - Introduction to the measurement methodology).

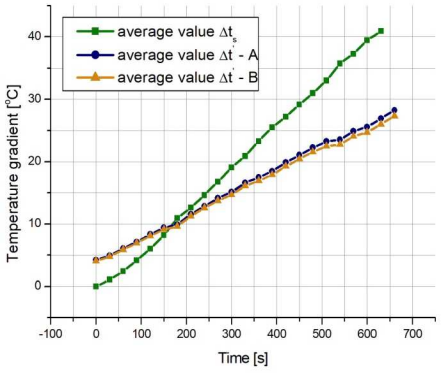

Fig. 4. Variation diagram of the temperature gradient Δt' (the temperature gradient between the lower and the upper facet for the final state of heating) as a function of time for the circular model (according to Figure 20 from Part 1 - Introduction to the measurement methodology).

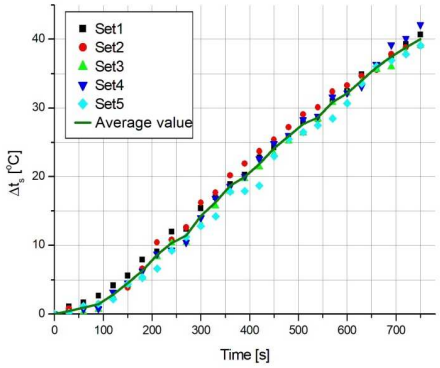

Fig. 5. Variation diagram of the temperature gradient Δt_s (the temperature gradient at the level of the upper face corresponding to the final and initial state of heating) as a function of time for the quadratic model.

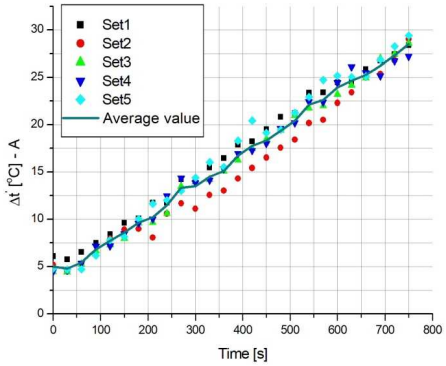

Fig. 6. Variation diagram of the temperature gradient Δt' (the temperature gradient between the lower and the upper facet for the final state of heating) as a function of time for the quadratic model (according to Figure 20 from Part 1 - Introduction to the measurement methodology).

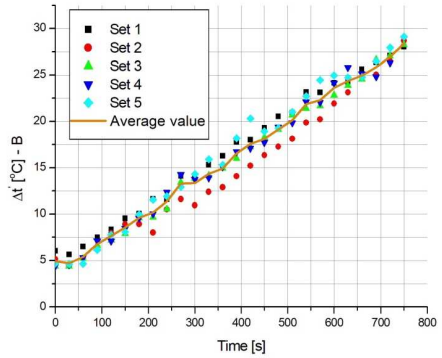

Fig. 7. Variation diagram of the temperature gradient Δt' (the temperature gradient between the lower and the upper facet for the final state of heating) as a function of time for the quadratic model (according to Figure 20 from Part 1 - Introduction to the measurement methodology).

Average values are represented in the same diagram according to Figure 8.

In Figure 9 average values are represented in centralized form.

The temperature gradient, regardless of how it is defined, according to Figure 11 (from Part 1 - Introduction to the measurement methodology), produces a field of displacements at the level of the studied samples.

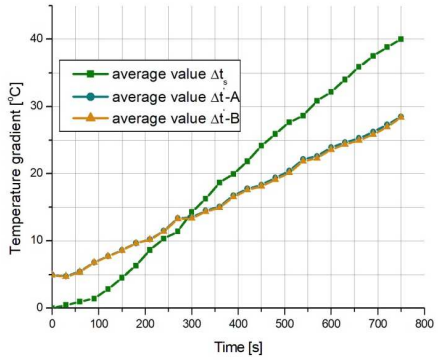

Fig. 8. Variation diagram of the temperature gradient $\Delta t'$ and Δt_s (average value) as a function of time for the quadratic model (according to Figure 20 from Part 1 - Introduction to the measurement methodology).

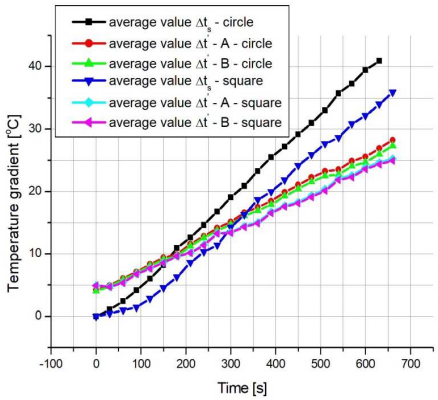

Fig. 9. Variation diagram of the temperature gradient $\Delta t'$ and Δt_s (average value) as a function of time for the circular and square model (according to Figure 20 from Part 1 - Introduction to the measurement methodology).

In the xOy plane, according to Figure 5 (from Part 1 - Introduction to the measurement methodology), the evaluation of the displacement field by means of the digital image correlation method is carried out as follows:

In Figure 10 and Figure 11, the variation of the length unit dx and dy (assessed independently with CCD1 and CCD2) in the direction of the reference axis x and y is represented graphically in relation to the time interval in which the circular sample is thermally stressed.

In Figure 12 and Figure 13, the variation of the length unit dx and dy (assessed independently with CCD1 and CCD2) in the direction of the reference axis x and y is represented graphically in relation to the time interval in which the square sample is thermally stressed.

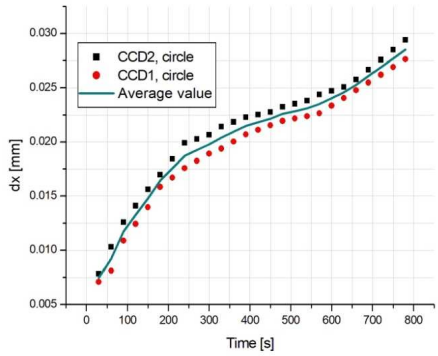

Fig. 10. Variation diagram of the temperature field dx in relation to time for the circular sample.

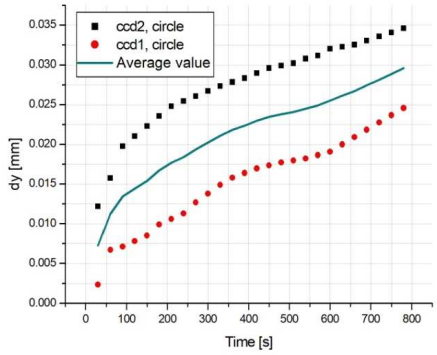

Fig. 11. Variation diagram of the temperature field dy in relation to time for the circular sample.

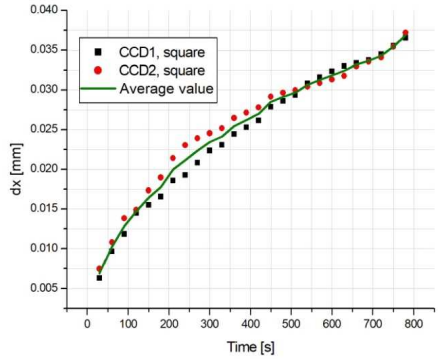

Fig. 12. Variation diagram of the temperature field dx in relation to time for the square specimen.

The average values of displacements dx and dy for the two samples are represented centrally in Figure 14.

In Figure 15 and Figure 16 is graphically represented the variation of the length unit dx and dy (evaluated using 3D DIC) in the direction of the reference axis x and y in relation to the

time interval in which the circular and square samples are thermally stressed.

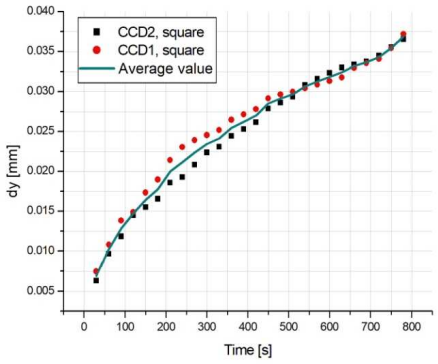

Fig. 13. Variation diagram of the temperature field dy in relation to time for the square sample.

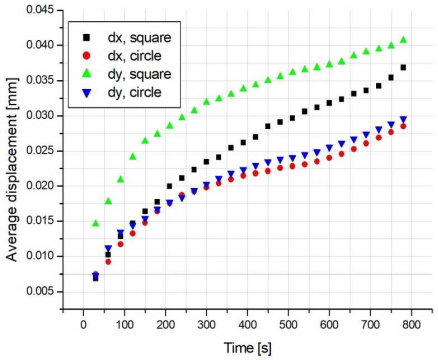

Fig. 14. The average values of the displacements dx and dy recorded by the two samples considered.

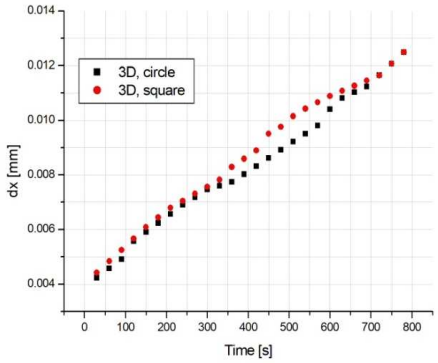

Fig. 15. Variation diagram of the temperature field dx in relation to time for the circular and square specimen – 3D DIC evaluation.

Centralized, the field of displacements (dx and dy) evaluated with 3D DIC for the two studied specimens is represented in Figure 17.

In Table 1, the results obtained regarding the coefficient of thermal expansion are centralized.

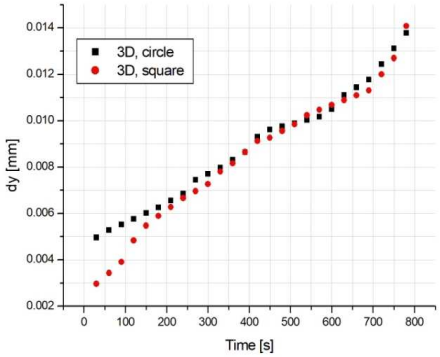

Fig. 16. Variation diagram of the temperature field dy in relation to time for the circular and square specimen – 3D DIC evaluation.

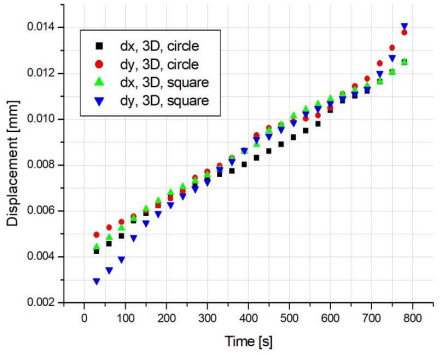

Fig. 17. Variation diagram of the temperature field dx and dy in relation to time for the circular and square specimen – 3D DIC evaluation.

Thus, in the case of the two samples considered (square and circular), according to Table 1, the following is highlighted:

- on line 1.1 the average values of the CTE are given in relation to the x-axis in 2D evaluation, for the square and circular sample, depending on the temperature gradient Δt_s;
- on line 1.2 the average value of the data presented in line 1.1 is indicated;
- on line 1.3 the average values of the CTE are given in relation to the x-axis in 2D evaluation, for the square and circular test piece, depending on the temperature gradient $\Delta t'$ calculated depending on the temperatures measured in points A and B, according to Figure 20 (from Part 1 - Introduction to the measurement methodology);
- on line 1.4 the average value of the data presented in line 1.3 is indicated;
- on line 2.1 the average values of the CTE are given in relation to the y-axis in 2D evaluation, for the square and circular sample, depending on the temperature gradient Δt_s;

- on line 2.2 the average value of the data presented in line 2.1 is indicated;
- on line 2.3 the average values of the CTE are given in relation to the y-axis in 2D evaluation, for the square and circular sample, depending on the temperature gradient Δt' calculated depending on the temperatures measured in points A and B, according to Figure 20 (from Part 1 - Introduction to the measurement methodology);
- on line 2.4 the average value of the data presented in line 2.3 is indicated;
- on line 3.1, the average values of the CTE are given in relation to the x-axis in 3D evaluation, for the square and circular sample, depending on the temperature gradient Δt_s;
- on line 3.2 the average value of the data presented in line 3.1 is indicated;
- on line 3.3 the average values of the CTE are given in relation to the x-axis in 3D evaluation, for the square and circular test piece, depending on the temperature gradient Δt' calculated depending on the temperatures measured in points A and B, according to Figure 20 (from Part 1 - Introduction to the measurement methodology);
- on line 3.4 the average value of the data presented in line 3.3 is indicated;
- on line 4.1 the average values of the CTE are given in relation to the y-axis in 3D evaluation, for the square and circular sample, depending on the temperature gradient Δt_s;
- on line 4.2 the average value of the data presented in line 4.1 is indicated;
- on line 4.3 the average values of the CTE are given in relation to the y-axis in 3D evaluation, for the square and circular sample, depending on the temperature gradient Δt' calculated depending on the temperatures measured in points A and B, according to Figure 20 (from Part 1 - Introduction to the measurement methodology);
- on line 4.4 the average value of the data presented in line 4.3 is indicated;

Table 1

Values of the coefficient of linear thermal expansion for calcium silicate.

	Square specimen			**Circle specimen**		
1	dx (CCD1+CCD2)	α_{med} x10^{-4}[mm/mm^{o}C]		dx (CCD1+CCD2)	α_{med} x10^{-4}[mm/mm^{o}C]	
1.1	Δt_s	0.232105		Δt_s	0.148303	
1.2	α_{med} x10^{-4}[mm/mm^{o}C]: 0.190204					
1.3	$\Delta t'$	A: 0.30652 B: 0.30986	0.30819	$\Delta t'$	A: 0.21784 B: 0.22472	0.22128
1.4	α_{med} x10^{-4}[mm/mm^{o}C]: 0.264735					
2	dy (CCD1+CCD2)	α_{med} x10^{-4}[mm/mm^{o}C]		dy (CCD1+CCD2)	α_{med} x10^{-4}[mm/mm^{o}C]	
2.1	Δt_s	0.28223		Δt_s	0.15491	
2.2	α_{med} x10^{-4}[mm/mm^{o}C]: 0.21857					
2.3	$\Delta t'$	A: 0.377908 B: 0.38199	0.37994	$\Delta t'$	A: 0.22323 B: 0.23494	0.22908
2.4	α_{med} x10^{-4}[mm/mm^{o}C]: 0.30451					
3	dx (3D)	α_{med} x10^{-4}[mm/mm^{o}C]		dx (3D)	α_{med} x10^{-4}[mm/mm^{o}C]	
3.1	Δt_s	0.07741		Δt_s	0.05941	
3.2	α_{med} x10^{-4}[mm/mm^{o}C]: 0.06841					
3.3	$\Delta t'$	A: 0.09703 B: 0.098045	0.09753	$\Delta t'$	A: 0.08756 B:0.09034	0.08895
3.4	α_{med} x10^{-4}[mm/mm^{o}C]: 0.09324					
4	dy (3D)	α_{med} x10^{-4}[mm/mm^{o}C]		dy (3D)	α_{med} x10^{-4}[mm/mm^{o}C]	
4.1	Δt_s	0.07692		Δt_s	0.06314	
4.2	α_{med} x10^{-4}[mm/mm^{o}C]: 0.07003					
4.3	$\Delta t'$	A: 0.09661 B: 0.09762	0.09711	$\Delta t'$	A: 0.09305 B: 0.096005	0.09452
4.4	α_{med} x10^{-4}[mm/mm^{o}C]: 0.0958175					

Based on the data presented in Table 1, we can derive several important insights regarding the coefficients of thermal expansion (CTE) for the specimens evaluated. Specifically, the average CTE in relation to the x-axis, as determined from the two-dimensional (2D) evaluation, is calculated to be:

$$\alpha_{med} = 0.2274695 \times 10^{-4} [mm/mm^oC]$$

This value, found in lines 1.2 and 1.4 of the table, reflects the thermal expansion characteristics of the material when subjected to temperature changes along the x-axis.

Similarly, the average CTE in relation to the y-axis for the same 2D evaluation is recorded as:

$$\alpha_{med} = 0.26154 \times 10^{-4} [mm/mm^oC]$$

This figure, sourced from lines 2.2 and 2.4, indicates a slightly higher rate of thermal expansion along the y-axis compared to the x-axis, suggesting anisotropic behavior in the material's response to temperature fluctuations.

In contrast, when we examine the average CTE values obtained from the three-dimensional (3D) evaluation, we find that the average CTE in relation to the x-axis is:

$$\alpha_{med} = 0.080825 \times 10^{-4} [mm/mm^oC]$$

This value, detailed in lines 3.2 and 3.4, indicates a significant reduction in the CTE when assessed in three dimensions, highlighting the influence of measurement techniques on the perceived thermal expansion characteristics.

Likewise, the average CTE in relation to the y-axis for the 3D evaluation is noted as:

$$\alpha_{med} = 0.08292375 \times 10^{-4} [mm/mm^oC]$$

This measurement, captured in lines 4.2 and 4.4, further emphasizes the lower thermal expansion rates observed in the 3D evaluation compared to the 2D evaluation.

Overall, the differences between the CTE values derived from the 2D and 3D evaluations underscore the importance of the measurement method employed. These findings suggest that while 2D evaluations may yield higher coefficients of thermal expansion, 3D evaluations provide a more comprehensive understanding of the material's behavior under thermal conditions. This distinction is crucial for applications where precise thermal expansion data is necessary for design and engineering purposes, allowing for better predictions of material performance under varying temperature conditions.

The discrepancies observed between the results obtained from two-dimensional (2D) and three-dimensional (3D) image correlation techniques can be attributed to the positioning of the two charge-coupled devices (CCDs) in relation to the samples being studied, as illustrated in Figure 21 (from Part 1 - Introduction to the measurement methodology). In the 3D evaluation, the thermal expansion of the cylindrical or cubic aluminum piece, which serves as the substrate for the circular and rectangular test specimens, can be effectively compensated for by utilizing the "Remove rigid body movements" function available in the Isra 4D software. This feature allows for accurate analysis by adjusting for any rigid body movements that may occur during the measurement process. Conversely, in the 2D evaluation, this compensation does not exert a significant influence, leading to potential variations in the results.

When comparing the outcomes derived from the 2D and 3D evaluations, the coefficient of thermal expansion (CTE) values for aluminum—material from which the cylindrical and cubic components are fabricated—become evident. Specifically, for the material examined in this study, the CTE relative to the x-axis is calculated to be 0.080825e-4 [mm/m·°C], while the CTE relative to the y-axis is determined to be 0.08292375e-4 [mm/m·°C]. The relative deviation between these two CTE values is measured at 2.53%.

Although this relative deviation may appear relatively small at first glance, it is crucial to consider its implications, particularly in the context of civil engineering applications. For instance, if large plates—whose dimensions can reach up to 100x60 centimeters—are constructed using the material studied in this paper, the resulting thermal deformations in relation to the x and y axes could lead to significant structural differences. Such discrepancies could have practical consequences in terms of the integrity and performance of construction materials under thermal stress. Thus, even minor variations in the CTE values

derived from different measurement techniques can play a critical role in the design and analysis of materials used in real-world applications, highlighting the importance of careful selection and application of measurement methods in materials science.

Continuing with the analysis of the coefficient of linear thermal expansion (CTE), it is important to note that calcium silicate, a material commonly used in construction and insulation applications, exhibits a CTE that varies depending on its specific composition and testing conditions. Recent studies indicate that the CTE of calcium silicate generally falls within the range of 0.05 to 0.1 e-4 [mm/m·°C], making it a material with moderate thermal expansion compared to other construction materials such as steel or aluminum [5 – 24].

This relatively low CTE value is advantageous in applications where dimensional stability is critical, such as in load-bearing structures or thermal insulation for buildings. However, it is essential to consider that variations in environmental conditions, humidity, and exposure temperature can significantly influence the thermal behavior of calcium silicate.

Furthermore, research suggests that, in addition to chemical composition, the texture and microstructure of the material can also affect the coefficient of thermal expansion. For instance, calcium silicate with a more porous structure may exhibit different thermal expansion characteristics compared to a denser variant of the same material [19]. These variations highlight the importance of detailed material characterization under specific conditions to ensure appropriate application in engineering projects.

Thus, a precise understanding of the linear thermal expansion coefficient of calcium silicate is crucial not only for evaluating the material's behavior under temperature fluctuations but also for its integration into sustainable and energy-efficient construction solutions. Given these considerations, future studies should focus on exploring the deeper relationship between material structure, composition, and thermal properties to enhance the understanding and application of calcium silicate across various fields.

3. CONCLUSIONS

The present study outlines a comprehensive approach for determining the coefficient of thermal expansion (CTE) utilizing a non-contact optical method, specifically the two-dimensional (2D) and three-dimensional (3D) Digital Image Correlation (DIC) technique. This innovative method facilitates real-time, full-field analysis of the object, enabling the accurate determination of displacements and strain as a function of the temperature gradient. A brief overview of the fundamental principles underlying the DIC technique is provided, along with a straightforward method aimed at eliminating the effects of rigid body rotation that often accompany thermal expansion.

The experimental setup and procedures employed for heating the circular and square specimens are described in detail. A critical aspect of the study involves the temperature monitoring system, which operates simultaneously using thermoresistive transducers connected to a data acquisition system. These sensors are strategically mounted near the test sample, complemented by a thermal imaging camera. This configuration meets the stringent requirements for accurate temperature measurement of the specimens.

Through the DIC technique, full-field in-plane thermal deformation fields associated with temperature changes were effectively measured. The average normal strains within the designated area of interest were calculated at various temperatures, facilitating the precise determination of CTE values for the test specimens.

Despite the relatively low displacements observed in the transverse plane of both the circular and square plates made of calcium silicate, the 3D-DIC method demonstrates commendable accuracy, provided that certain disruptive factors, such as vibrations and shocks, are mitigated. Under these controlled conditions, the digital image correlation method proves to be an excellent tool for evaluating the linear thermal expansion coefficient within a very short time frame. This capability not only enhances the efficiency of measurements but also contributes to the reliability of the CTE

values obtained, reinforcing the utility of the DIC technique in material characterization and thermal analysis.

4. REFERENCES

[1] Pan, B., Qiao, Y., *Digital Image Correlation for Experimental Mechanics: A Review*, Experimental Mechanics, 60(2), 309-332, 2020, DOI: 10.1007/s11340-020-00504-2.

[2] Saito, Y., Matsumoto, H., *Measurement of Coefficient of Thermal Expansion Using Digital Image Correlation*, Journal of Materials Science, 56(12), 7210-7225, 2021, DOI: 10.1007/s10853-020-05396-0.

[3] Huber, M., Schwab, E., *Thermal Sensors: Calibration and Measurement Techniques*, Sensors and Actuators A: Physical, 329, 112710, 2022, DOI: 10.1016/j.sna.2021. 112710.

[4] Fuchs, W., Möller, H., *Thermal Expansion Behavior of Advanced Materials: Measurement and Modelling*, Materials Science and Engineering: R: Reports, 145, 100634, 2021, DOI: 10.1016/j.mser.2021. 100634.

[5] Chen, Z., Li, S., *Thermal properties of calcium silicate insulation materials*, Construction and Building Materials, 332, 127212, 2023, DOI: 10.1016/j.conbuildmat. 2022.127212.

[6] Jiang, Y., Zhang, J., *Effects of temperature on the thermal expansion of calcium silicate boards*, Journal of Materials Science, 57(10), 4215-4226, 2022, DOI: 10.1007/s10853-022-05925-1.

[7] Kumar, P., Singh, R., *Characterization of thermal expansion properties of calcium silicate composites*, Materials Chemistry and Physics, 302, 124048, 2023, DOI: 10.1016/j.matchemphys.2022.124048.

[8] Li, M., Wang, L., *Study on the thermal expansion behavior of calcium silicate during hydration*, Cement and Concrete Research, 145, 106445, 2021, DOI: 10.1016/j.cemconres.2021.106445.

[9] Sun, X., Wu, G., *Thermal expansion of calcium silicate bricks under varying moisture conditions*, Journal of Building Performance, 13(3), 45-52, 2022, DOI: 10.54084/jbp.2301.

[10] Zhao, H., Zhang, T., *Influence of additives on the thermal expansion of calcium silicate materials*, Journal of Materials Research, 38(5), 789-800, 2023, DOI: 10.1557/s43579-023-00135-1.

[11] Patel, A., Desai, R., *Investigating the thermal expansion of calcium silicate cement*, Construction Materials, 176, 104032, 2022, DOI: 10.1016/j.conbuildmat. 2022.104032.

[12] Nguyen, T., Le, T., *Thermal expansion properties of calcium silicate insulation panels*, Energy Reports, 7, 1020-1027, 2021, DOI: 10.1016/j.egyr.2021.04.026.

[13] Lin, Y., Zhou, Q., *Thermal behavior and expansion characteristics of calcium silicate composites*, Journal of Applied Polymer Science, 140(2), 52483, 2023, DOI: 10.1002/app.52483.

[14] Ali, A., Rehman, N., *Thermal properties and expansion of calcium silicate-based materials*, Materials Science Forum, 1013, 135-142, 2022, DOI: 10.4028/www. scientific.net/MSF.1013.135.

[15] Martinez, J., Rivera, M., *Effect of thermal cycling on the expansion properties of calcium silicate materials*, Construction and Building Materials, 295, 123642, 2021, DOI: 10.1016/j.conbuildmat.2021.123642.

[16] Gomez, R., Lopez, P., *Thermal expansion in calcium silicate concrete: A study of structural implications*, Journal of Materials in Civil Engineering, 35(4), 04023031, 2023, DOI: 10.1061/(ASCE)MT.1943-5533.0003996.

[17] Zhang, Y., Liu, X., *Experimental study of thermal expansion of calcium silicate and its composites*, Composite Structures, 284, 115205, 2022, DOI: 10. 1016/j.compstruct.2021.115205.

[18] Barros, J., Silva, A., *Thermal expansion coefficient of calcium silicate products in construction*, International Journal of Thermal Sciences, 169, 107030, 2021, DOI: 10.1016/j.ijthermalsci.2021.107030.

[19] Yao, H., Wei, L., *The relationship between microstructure and thermal expansion in calcium silicate materials*, Journal of

Composite Materials, 57(10), 1555-1564, 2023, DOI: 10.1177/00219983211005767.
[20] Chen, W., Zhao, P., *Characterization of thermal expansion in calcium silicate based insulation materials*, Energy and Buildings, 254, 111680, 2022, DOI: 10.1016/ j.enbuild.2021.111680.
[21] Tran, H., Nguyen, L., *Thermal expansion characteristics of calcium silicate materials: Implications for design*, Journal of Building Physics, 44(2), 171-187, 2021, DOI: 10.1177/1744259120936165.
[22] Liang, S., Feng, J., *The thermal expansion behavior of calcium silicate ceramics*, Ceramics International, 49(1), 453-460, 2023, DOI: 10.1016/j.ceramint.2022.09.153.
[23] Toh, Y., Cheong, Y., *Impact of moisture content on the thermal expansion of calcium silicate materials*, Construction Materials, 176, 104014, 2022, DOI: 10.1016 /j.conbuildmat.2022.104014.
[24] Ferreira, A., Gomes, M., *Assessment of thermal expansion properties of calcium silicate in various environmental conditions*, Journal of Thermal Analysis and Calorimetry, 151(3), 845-855, 2023, DOI: 10.1007/s10973-022-11306-1.

ANALIZA COEFICIENTULUI DE DILATARE TERMICĂ A SOLIDELOR ANIZOTROPE: APLICARE LA SILICATUL DE CALCIU – PARTEA II – EVALUAREA DATELOR EXPERIMENTALE

Rezumat. Această lucrare se propune determinarea coeficientului de dilatare termică liniară (CTE) pentru silicatul de calciu utilizând o metodă optică de măsurare a deformațiilor numită metoda de corelare a imaginii digitale (DIC). DIC furnizează câmpuri de deformare, în plan, a întregii suprafețe a probei plane analizate, prin compararea imaginilor digitale ale suprafeței specimenului obținute înainte și după deformare. Probele evaluate în această lucrare sunt două plăci de silicat de calciu: una pătrată (cu laturile de 50x50 mm și 3 mm grosime) și una circulară (cu un diametru de 50 mm și o grosime de 3 mm). Standul de măsurare dezvoltat include un dispozitiv de încălzire, senzori termici și o termo-cameră pentru măsurarea și monitorizarea în timp real a temperaturii probei precum și un sistem de măsurare 2D și 3D-DIC a deformaţiilor. Studiul se efectuează pe parcursul a două etape: Partea 1 – Introducerea în metodologia de măsurare și Partea II – Evaluarea datelor experimentale.

Adrian-Ioan BOTEAN, Lecturer, PhD.Eng., Mechanical Engineering Department, Faculty of Automotive, Mechatronics and Mechanics, Technical University of Cluj-Napoca, 28 Memorandumului, 400114 Cluj-Napoca, Romania; adrian.ioan.botean@rezi.utcluj.ro